**References and Notes**

1. G. K. H. Shimizu, *J. Solid State Chem.* **178**, 2519 (2005).
2. R. Kitaura, K. Seki, G. Akiyama, S. Kitagawa, *Angew. Chem. Int. Ed.* **42**, 428 (2003).
3. T. Loiseau *et al.*, *Chem. Eur. J.* **10**, 1373 (2004).
4. G. J. Halder, C. J. Kepert, *J. Am. Chem. Soc.* **127**, 7891 (2005).
5. K. Hanson, N. Calin, D. Bugaris, M. Scancella, S. C. Sevov, *J. Am. Chem. Soc.* **126**, 10502 (2004).
6. P. D. C. Dietzel, B. Panella, M. Hirscher, R. Blom, H. Fjellvåg, *Chem. Commun.* **2006**, 959 (2006).
7. E. Y. Lee, S. Y. Jang, M. P. Suh, *J. Am. Chem. Soc.* **127**, 6374 (2005).
8. C.-L. Chen, A. M. Goforth, M. D. Smith, C.-Y. Su, H.-C. zur Loye, *Angew. Chem. Int. Ed.* **44**, 6673 (2005).
9. D. Maspoch *et al.*, *Nat. Mater.* **2**, 190 (2003).
10. L. G. Beauvais, M. P. Shores, J. R. Long, *J. Am. Chem. Soc.* **122**, 2763 (2000).
11. H. Li, C. E. Davis, T. L. Groy, D. G. Kelley, O. M. Yaghi, *J. Am. Chem. Soc.* **120**, 2186 (1998).
12. K. Takaoka, M. Kawano, M. Tominaga, M. Fujita, *Angew. Chem. Int. Ed.* **44**, 2151 (2005).
13. J. L. Atwood, L. J. Barbour, A. Jerga, B. L. Schottel, *Science* **298**, 1000 (2002).
14. D. J. Chesnut *et al.*, *Coord. Chem. Rev.* **190–192**, 737 (1999).
15. Materials and methods are available as supporting material on *Science* Online.
16. L. Carlucci, G. Ciani, D. M. Proserpio, A. Sironi, *J. Chem. Soc. Dalton Trans.* **1997**, 1801 (1997).
17. A. L. Spek, PLATON (University of Utrecht, Utrecht, Netherlands, 1999).
18. Cycling between **1** and **1′** (via formation of the rehydrated phase **1″** by exposure of the outgassed material to laboratory air), followed by further outgassing and $CO_2$ uptake, reveals that the porosity remains [BET surface area for cycle 2 is 217(4) $m^2/g$], confirming the reversibility of the substitution reaction.
19. X. Zhao *et al.*, *Science* **306**, 1012 (2004).
20. D. Hagrman, R. P. Hammond, R. Haushalter, J. Zubieta, *Chem. Mater.* **10**, 2091 (1998).


21. We thank the Engineering and Physical Sciences Research Council (EPSRC) for funding under grant EPSRC/C511794 and access to the Synchotron Radiation Source. We thank B. Carter and S. Masaoka for assistance with the synchrotron experiments. The Intelligent Gravimetric Analyzer instrument is funded by the EPSRC Molecular Materials Centre. Crystallographic data have been submitted to the Cambridge Crystallographic Database with reference numbers CCDC-617201 (**1**) and CCDC-617202 (**1′**) and are available free of charge at www.ccdc.cam.ac.uk/data_request/cif.


**Supporting Online Material**

www.sciencemag.org/cgi/content/full/315/5814/977/DC1
Materials and Methods
Figs. S1 to S9

22 September 2006; accepted 13 December 2006
10.1126/science.1135445

# Magmatic and Crustal Differentiation History of Granitic Rocks from Hf-O Isotopes in Zircon

**A. I. S. Kemp,[1,2]* C. J. Hawkesworth,[1] G. L. Foster,[1] B. A. Paterson,[1] J. D. Woodhead,[3] J. M. Hergt,[3] C. M. Gray,[4] M. J. Whitehouse[5]**

**Granitic plutonism is the principal agent of crustal differentiation, but linking granite emplacement to crust formation requires knowledge of the magmatic evolution, which is notoriously difficult to reconstruct from bulk rock compositions. We unlocked the plutonic archive through hafnium (Hf) and oxygen (O) isotope analysis of zoned zircon crystals from the classic hornblende-bearing (I-type) granites of eastern Australia. This granite type forms by the reworking of sedimentary materials by mantle-like magmas instead of by remelting ancient metamorphosed igneous rocks as widely believed. I-type magmatism thus drives the coupled growth and differentiation of continental crust.**

Earth's veneer of continental crust is unique among the known terrestrial planets and attests to a distinctive mode of planetary differentiation (*1*). The vast granitic batholiths and their erupted analogs that dominate continental landmasses are an obvious manifestation of such differentiation. Yet how granites relate to crustal growth processes remains puzzling, because the majority of these rocks have isotope signatures that preclude a direct mantle ancestry (*2*–*6*). The paradigm from studies in the Lachlan Fold Belt (eastern Australia) is that granitic magmas derive from preexisting sources that are fundamentally either supracrustal (formed originally at Earth's surface) or infracrustal (igneous rocks that solidified at depth) in character, as reflected in the S- and I-type notation used to describe them (*7*). Granites of I-type affinity are globally prevalent. A corollary of the I-S type concept is that the isotope compositions of granites reflect the crustal residence prehistory of their protoliths (*4*), constraining the age and architecture of the deep crust as well as the timing of ancient crust-forming episodes. In contrast, other studies attribute the isotope variations to interaction between older crust and mantle-derived magma (*2*, *5*, *6*, *8*), implying that crustal growth is intrinsic to granitic emplacement. Mixing models are controversial (*9*), because ascertaining the timing and magnitude of mantle input is impeded by difficulties with retrieving the record of magmatic evolution from bulk granite compositions. This record is, however, preserved within the chemical and isotope stratigraphy of certain minerals (*10*–*13*). The robust accessory mineral zircon has the advantage that its intricate growth zoning can be dated by U-Pb isotopes, and it tracks changing melt chemistry in its Hf and O isotope ratios (*13*, *14*). We report an integrated in situ U-Pb, Hf, and O isotope study of zircons from granites, in this case the Lachlan I-types, to decipher the crustal evolutionary processes attending silicic magmatism.

We examined zircon crystals from three granitic suites (groups of rocks related through common geochemical trends): Jindabyne [415 million years ago (Ma)], Why Worry (400 Ma), and Cobargo (390 Ma). The Jindabyne plutons intrude Silurian (~425 Ma) S-type granites, whereas the Why Worry and Cobargo rocks are emplaced into Ordovician metasedimentary units at a depth of around 10 to 12 km. Rocks of each granitic suite have hallmark I-type features in their abundance of hornblende and in having higher concentrations of Ca, Na, and Sr than do S-type granites of similar silica content (*7*). Samples at either end of the compositional range of each suite were targeted. Zircons were also separated from a mafic rock associated with each suite, these being a gabbro (Jindabyne), synplutonic dolerite dyke (Why Worry), and diorite enclave (Cobargo). The mafic rocks are coeval with the respective granitic suites and share the same distinctive chemical features (*15*, *16*), implying consanguinity.

The zircons of all samples were first dated by ion microprobe U-Pb isotope analysis (table S1). This identified a minor inherited (pre-magmatic) component in some samples (*15*), but the discussion below focuses on data obtained from the magmatic portion of each zircon. O isotope compositions ($^{18}O/^{16}O$, expressed as $\delta^{18}O$) (*17*) were determined from the same zircon growth zone using a Cameca IMS 1270 ion microprobe (*18*) (table S2). Unlike bulk rock samples, zircon is extremely retentive of the magmatic O isotope ratio (*19*), and zircons in equilibrium with pristine mantle-derived melts have a narrow range of $\delta^{18}O$ [5.3 ± 0.3 per mil (‰)] (*14*). This range is insensitive to magmatic differentiation, because the attendant rise in bulk rock $\delta^{18}O$ is compensated for by an increase in zircon/liquid $\delta^{18}O$ fractionation from +0.5‰ for mafic melts to +1.5‰ for silicic derivatives (*14*). Values of $\delta^{18}O$ in zircon above 5.6‰ thus fingerprint an $^{18}O$-enriched supracrustal component in the magma from which the zircon crystallized, this being either sedimentary rock (10 to 30‰) or altered volcanic rock (to 20‰) (*20*). The $^{176}Hf/^{177}Hf$ ratios were measured by laser

[1]Bristol Isotope Group, Earth Sciences Department, University of Bristol, Bristol BS8 1RJ, UK. [2]School of Earth and Environmental Sciences, James Cook University, Townsville, 4811, Australia. [3]School of Earth Sciences, University of Melbourne, Victoria, 3010, Australia. [4]Centre for Theoretical Isotope Studies, Greensborough, Victoria, 3088, Australia. [5]Swedish Museum of Natural History, Box 50007, SE-104 05 Stockholm, Sweden.

*To whom correspondence should be addressed. E-mail: tony.kemp@jcu.edu.au

ablation multicollector inductively coupled plasma mass spectrometry (*18*) (table S3), targeting, wherever possible, the pits generated by ion microprobe analysis.

An important feature of the Hf isotope data (Fig. 1) is the spectrum of εHf values exhibited by zircons of the same rock (up to 10 ε units) (*21*). Such variations within a single sample can only be reconciled by the operation of open-system processes that are capable of shifting the $^{176}Hf/^{177}Hf$ ratio of the melt from which the zircons precipitated. To identify these processes, it is necessary to deduce the polarity of Hf isotope change during zircon growth. This can be accomplished by examination of intracrystal isotope zoning trends and by pairing the isotope variations with trace element ratios (such as Th/U) that are proxies for the degree of differentiation. In cases where isotope zoning is pronounced, $^{176}Hf/^{177}Hf$ generally decreases toward zircon rims, although some grains show the opposite pattern. Trace element microanalysis has established that Th/U ratios typically fall from core to rim in the studied zircons (table S1), and the εHf values of the zircons also decrease systematically with Th/U (Fig. 2). We interpret this as evidence for a progressive reduction in the $^{176}Hf/^{177}Hf$ ratio during the magmatic evolution of each suite, as would be induced by the addition of an unradiogenic (continental crust–like) component. The reversely zoned zircons manifest episodic input from material with higher εHf values.

Coupling the $^{176}Hf/^{177}Hf$ ratios of the zircons with their O isotope compositions reveals the nature of the crustal component. Zircons of individual samples exhibit a $\delta^{18}O$ range of 2 to 4‰, and, although rarely resolvable, intragrain heterogeneity can exceed 1‰ and involves a rise in $\delta^{18}O$ from core to rim (table S2). εHf and $\delta^{18}O$ are correlated for zircons of each suite and define curved arrays that extend to much higher $\delta^{18}O$ values than those of zircons precipitated from mantle melts (Fig. 3). These elevated $\delta^{18}O$ values diagnose a substantial supracrustal component in the Lachlan I-type granites. The isotope array defined by zircons of each suite has a distinctive trajectory anchored by a different low-$\delta^{18}O$ end member that is in equilibrium with mantle O. For Jindabyne and Why Worry, this corresponds to zircons of the associated mafic intrusives. At higher $\delta^{18}O$ values, the arrays converge toward the field defined by magmatic zircons of S-type granites and the inferred Hf-O isotope composition of the metasedimentary country rocks.

The covariant εHf- $\delta^{18}O$ zircon arrays are therefore tracking the progressive interaction between two end-member components during zircon crystallization, these being parental low-$\delta^{18}O$ magmas and metasedimentary-derived materials. Such interaction could involve either mixing and hybridization with crustal partial melts or the digestion of supracrustal rock (assimilation) by low-$\delta^{18}O$ magmas. The origin of the low-$\delta^{18}O$ magmas is not uniquely constrained by the zircon isotope arrays. The data are permissive of an enriched mantle heritage or an infracrustal progenitor, or of variable combinations of the two (*8*). A predominantly mantle derivation accords with the mafic character of the inferred low-$\delta^{18}O$ components. These mafic magmas were subsequently modified by crustal contamination, as is evident in the spread of zircon εHf and $\delta^{18}O$ values in the Jindabyne gabbro and Why Worry basalt (Fig. 3), but zircon crystallized sufficiently early to retain vestiges of the original isotope signature.

Although long suspected (*5*), a mixed and partly supracrustal source for the Lachlan I-type granites is now incontrovertible. Major supracrustal input has also recently been inferred for other $^{18}O$-enriched circum-Pacific I-type plutons (*22*). The remaining task is to quantify the metasedimentary component of each Lachlan suite and to determine the conditions under which this was incorporated. Assuming that assimilation-fractional crystallization equations (*23*) are a reasonable approximation of magmatic evolution, most zircons in the Cobargo Suite

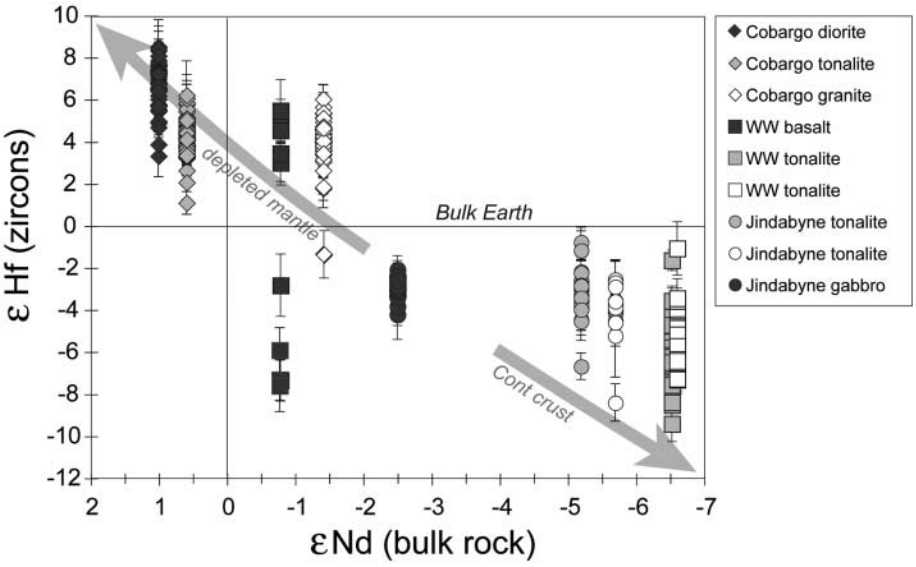


**Fig. 1.** The Hf isotope composition of melt-precipitated zircons from samples of each suite as a function of whole-rock Nd isotope composition at the time of crystallization (WW, Why Worry). Error bars represent 2 SEM.

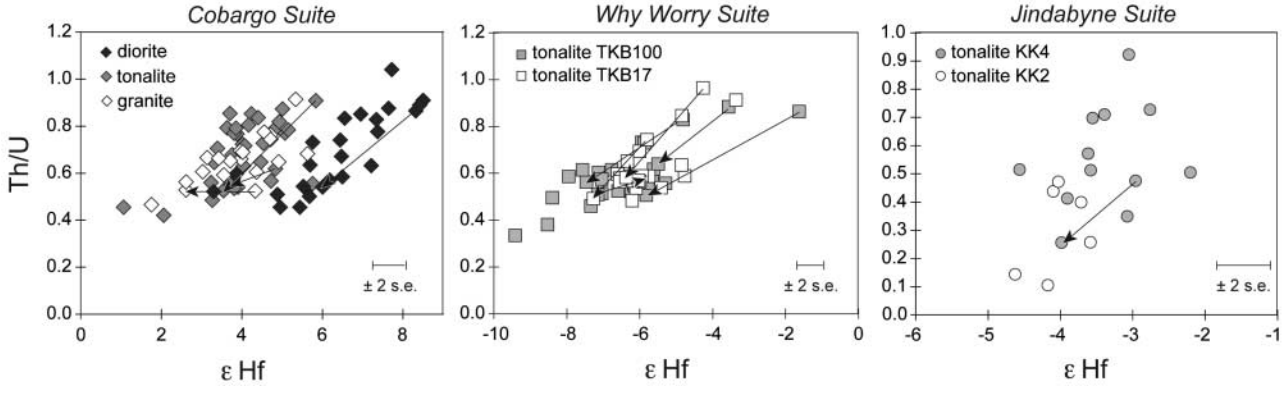


**Fig. 2.** Hf isotopic compositions of zircons from each suite plotted against the Th/U ratio measured for the same part of the crystal. Arrowed lines show the sense of core-to-rim zonation for individual zircons.

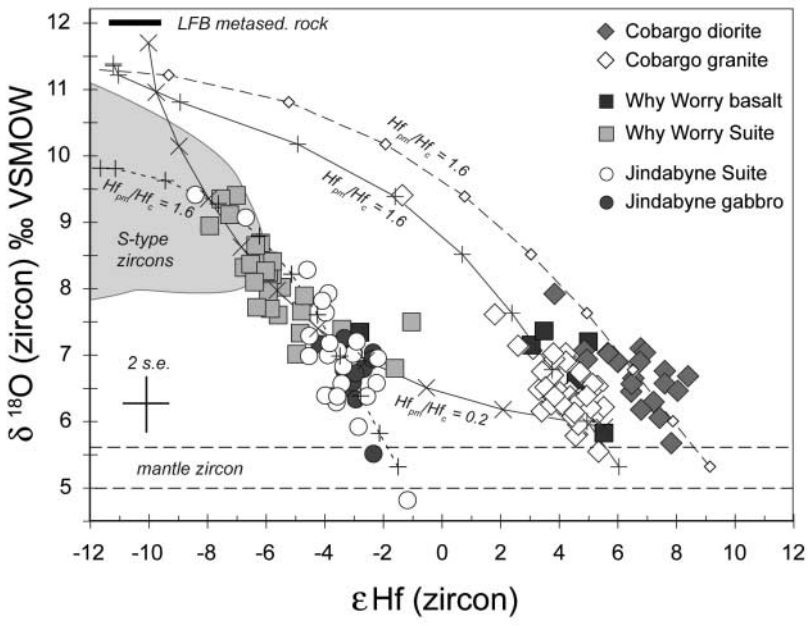


**Fig. 3.** Plot of $\delta^{18}O$ versus εHf for zircons of this study, showing the putative curves corresponding to magma evolution by crustal assimilation-crystallization (AFC) (*23*). Data from samples of each suite are assigned the same symbol (error bars depict the average 2 SEM uncertainty). The $\delta^{18}O$ value of Lachlan metasedimentary rock is taken from (*33*), and the shaded field depicts the isotope compositions of zircons from the Lachlan S-type granites. Ticks on the curves represent 10% AFC increments, and the ratio of Hf concentrations in the parental magma (pm) and crustal (c) end members ($Hf_{pm}/Hf_c$) is indicated for each. VSMOW, Vienna standard mean ocean water; LFB metased. rock, Lachlan Fold Belt metasedimentary rock.

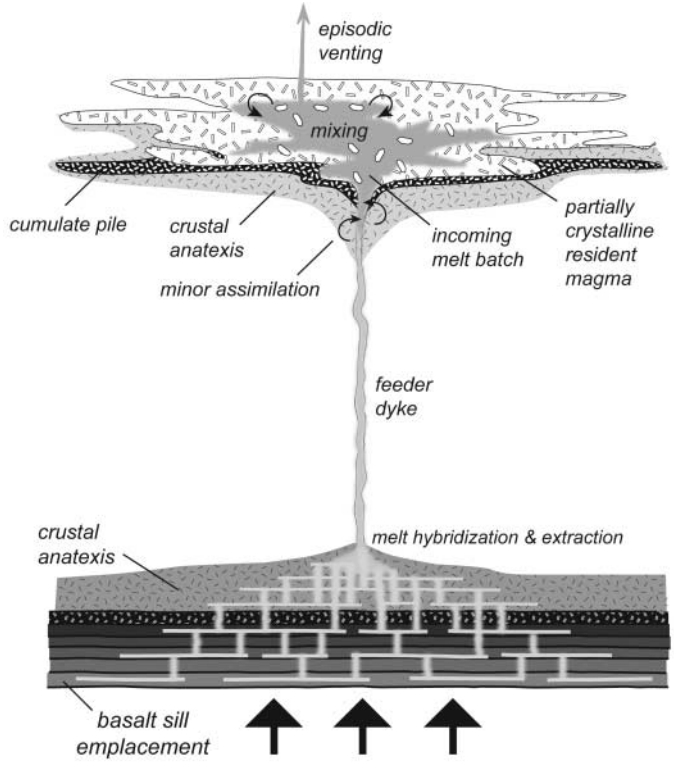


**Fig. 4.** A schematic model for the formation of I-type granites in eastern Australia, based on the analysis of Hf-O isotopes in zircon. Silicic melts are generated at depth through interaction between residual liquids from basalt crystallization and melts derived from the overlying supracrustal assemblage (*29*). These hybrid magmas are extracted to ascend and pond in the shallow crust to crystallize zircons whose isotopic signature records the progress of supracrustal incorporation at depth. Mingling and amalgamation of melt batches during protopluton assembly accumulate zircons with different isotope characteristics. Basaltic emplacement is localized at the interface between the mafic (oceanic) substrate to the eastern Lachlan Fold Belt and the overlying turbidite pile; the interface is likely to represent a substantial rheological contrast.

precipitated from melts containing up to 25% supracrustal material, the corresponding figures being around 40% for Jindabyne and 60% for Why Worry (Fig. 3 and supporting online text). The geometry of the εHf-$\delta^{18}O$ arrays places additional constraints on the mixing or assimilation process, because the curvature of these arrays is controlled by the relative Hf concentrations of the end members. For Cobargo and Jindabyne, the Hf content of the low-$\delta^{18}O$ magma must have exceeded that of the crustal component, as would be the case if the latter were a partial melt with residual zircon. Conversely, the concave-up trend defined by the Why Worry suite zircons requires that the supracrustal ingredient had the higher Hf concentration, which is consistent with bulk assimilation. Partially disaggregated metasedimentary enclaves in these plutons provide evidence for this process (*15*).

Petrogenetic models for the Lachlan I-type granites must reconcile two key aspects of the new data. First, the Hf-O isotope arrays extend to mantle-like values, indicating that zircon crystallization commenced before the ingestion of supracrustal material. However, the initial temperatures of the parental low-$\delta^{18}O$ magmas were inevitably higher than the zircon stability field, typically <800°C (*24*), and crustal incorporation is more effective for hot liquid magmas (*25*). We therefore infer that crustal assimilation and zircon precipitation occurred at different temperatures, and thus crustal levels, for part of the magmatic history. Second, the diversity of εHf and $\delta^{18}O$ values indicates that zircons of each granite sampled radically different melt compositions, yet they are now juxtaposed within the same rock volume. This demands a process in the plutonic environment that can unite crystals with disparate petrogenetic histories. Many volcanic rocks also comprise aggregates of crystals formed at different times from evolving melt compositions (*10*, *12*, *26*).

The following scenario is proposed (Fig. 4), accommodating the view that plutons are assembled incrementally (*27*, *28*). We envisage a dynamic dual-level process involving the incomplete solidification of basaltic magmas in a deep crustal hot zone (<35 to 40 km, constrained by the absence of a garnet signature in the Lachlan I-types), with batches of differentiated melt being extracted to ascend, coalesce, and crystallize in shallow magma reservoirs (*29*, *30*). The isotope systematics of each melt aliquot reflect the parental basalt composition and the degree of supracrustal input, this commencing at depth before zircon saturation and continuing to higher crustal levels where zircon begins to crystallize (Fig. 4). Thermal simulations predict increased crustal anatexis with hot zone maturation (*29*), promoting higher rates of metasedimentary rock assimilation by the crystallizing basalts with time (*25*) and greater blending between the basalt-derived liquids and crustal melts draining the hot zone.

Successive infusions of hybrid melt into the nascent pluton would therefore precipitate zircons with higher $\delta^{18}O$ and lower εHf values, as recorded by the zircon isotope arrays. Zircons with disparate isotope signatures are juxtaposed by mingling and crystal exchange between melt batches during pluton assembly and intrareservoir crystal-liquid sorting (*27*, *31*). Mixing with the recharge melt would also drive the resident magma and its crystallizing zircon cargo toward higher $\delta^{18}O$ and lower εHf values, explaining the intrazircon isotope zoning. Isotopic reversals in some zircons and basalt injection in the Why Worry plutons suggest that this evolution was punctuated by juvenile magma replenishments.

The refined view of granite genesis captured by the zircon isotope data compels a reappraisal of the I-S type concept and its implications for crustal evolution. In revealing the reworking of supracrustal material by juvenile magmas, our study suggests that I-type magmatism critically involves continental growth, this being camouflaged to some extent by the non–mantle-like isotope ratios of the bulk rocks. The overall proportion of new material added by the Lachlan I-type suites was near 85% for Cobargo, 70% for Jindabyne, and 50% for Why Worry. These estimates imply that Phanerozoic crust generation rates may have been higher than hitherto appreciated from studies of plutonic terranes (*6*, *32*), modifying global continental growth curves through time.

**References and Notes**


1. I. H. Campbell, S. R. Taylor, *Geophys. Res. Lett.* **10**, 1061 (1983).
2. D. J. DePaolo, *Science* **209**, 684 (1980).
3. P. J. Hamilton, R. K. O'Nions, R. J. Pankhurst, *Nature* **287**, 279 (1980).
4. M. T. McCulloch, B. W. Chappell, *Earth Planet. Sci. Lett.* **58**, 51 (1982).
5. C. M. Gray, *Earth Planet. Sci. Lett.* **70**, 47 (1984).
6. B.-M. Jahn, F. Wu, B. Chen, *Trans. R. Soc. Edinb. Earth Sci.* **91**, 181 (2001).
7. A. J. R. White, B. W. Chappell, *Tectonophysics* **43**, 7 (1977).
8. S. M. Keay, W. J. Collins, M. T. McCulloch, *Geology* **25**, 307 (1997).
9. B. W. Chappell, *J. Petrol.* **37**, 449 (1996).
10. J. P. Davidson, F. J. T. Tepley, *Science* **275**, 826 (1997).
11. T. E. Waight, R. Maas, I. A. Nicholls, *Contrib. Miner. Petrol.* **139**, 227 (2000).
12. J. R. Vazquez, M. R. Reid, *Science* **305**, 991 (2004).
13. W. L. Griffin *et al.*, *Lithos* **61**, 237 (2002).
14. J. W. Valley *et al.*, *Contrib. Mineral. Petrol.* **150**, 561 (2005).
15. A. I. S. Kemp, M. J. Whitehouse, C. J. Hawkesworth, M. K. Alarcon, *Contrib. Mineral. Petrol.* **150**, 230 (2005).
16. R. Hine, I. S. Williams, B. W. Chappell, A. J. R. White, *J. Geol. Soc. Aust.* **25**, 219 (1978).
17. The $\delta^{18}O$ notation signifies deviation of the measured $^{18}O/^{16}O$ value from Vienna standard mean ocean water in parts per thousand.
18. Materials and methods are available as supporting material on *Science* Online.
19. W. H. Peck, J. W. Valley, C. M. Graham, *Am. Mineral.* **88**, 1003 (2003).
20. J. M. Eiler, *Rev. Mineral.* **43**, 319 (2001).
21. The epsilon notation signifies deviation of the isotope ratio ($^{176}Hf/^{177}Hf$ and $^{143}Nd/^{144}Nd$) from a chondritic reference in parts per ten thousand.
22. J. S. Lackey, J. W. Valley, J. B. Saleeby, *Earth Planet. Sci. Let* **235**, 315 (2005).
23. D. J. DePaolo, *Earth Planet. Sci. Lett.* **53**, 189 (1981).
24. J. W. Valley, A. J. Cavosie, B. Fu, W. H. Peck, S. A. Wilde, *Science* **312**, 1139a (2006).
25. A. B. Thompson, L. Matile, P. Ulmer, *J. Petrol.* **43**, 403 (2002).
26. C. J. Hawkesworth, S. Turner, R. George, G. Zellmer, *Earth Planet. Sci. Let* **218**, 1 (2004).
27. R. A. Wiebe, W. J. Collins, *J. Struct. Geol.* **20**, 1273 (1998).
28. A. F. Glazner, J. M. Bartley, D. S. Coleman, W. Gray, R. Z. Taylor, *GSA Today* **14**, 4 (2004).
29. C. Annen, J. D. Blundy, R. S. J. Sparks, *J. Petrol.* **47**, 505 (2005).
30. M. D. Jackson, M. J. Cheadle, M. P. Atherton, *J. Geophys. Res.* **108**, 2332 (2003).
31. S. Couch, R. S. J. Sparks, M. R. Carroll, *Nature* **411**, 1037 (2001).
32. C. J. Hawkesworth, A. I. S. Kemp, *Nature* **443**, 811 (2006).
33. J. R. O. Neil, B. W. Chappell, *J. Geol. Soc. London* **133**, 559 (1977).


34. We are indebted to J. Craven for guidance with oxygen isotope analysis at the Edinburgh Ion Microprobe Facility and to C. Coath for assistance with Hf isotope analysis at Bristol. R. Arculus, N. Pearson, and C. Graham generously provided advice at the outset of the study. Constructive comments by S. Sparks, B. Collins, and two reviewers are gratefully acknowledged. Funded by NERC grants NER/I/S/00942 and IMP/250/505.


**Supporting Online Material**

www.sciencemag.org/cgi/content/full/315/5814/980/DC1
Materials and Methods
SOM Text
Tables S1 to S5
References

11 October 2006; accepted 11 January 2007
10.1126/science.1136154

# Fracture-Controlled Paleo-Fluid Flow in Candor Chasma, Mars

**Chris H. Okubo* and Alfred S. McEwen**

**Color observations from the High Resolution Imaging Science Experiment on board the Mars Reconnaissance Orbiter reveal zones of localized fluid alteration (cementation and bleaching) along joints within layered deposits in western Candor Chasma, Mars. This fluid alteration occurred within the subsurface in the geologic past and has been exposed at the surface through subsequent erosion. These findings demonstrate that fluid flow along fractures was a mechanism by which subsurface fluids migrated through these layered deposits. Fractured layered deposits are thus promising sites for investigating the geologic history of water on Mars.**

The High Resolution Imaging Science Experiment (HiRISE) camera (*1*, *2*) on board the Mars Reconnaissance Orbiter (MRO) has returned images of the surface of Mars that have exceptional clarity and resolution. One of the first images of Mars returned by HiRISE in the low (250 to 315 km) mapping orbit is of the layered deposits within western Candor Chasma (Fig. 1 and fig. S1), one of the larger canyons of the Valles Marineris system, in the western equatorial region of Mars (fig. S2). Surface features ≳0.26 m (equivalent to one pixel) are detectable, and the shapes of objects ≳0.78 m across are resolved (*2*).

The layered deposits appear as alternating light- and dark-toned bands (Fig. 1 and fig. S1) and may be volcanic, eolian, or lacustrine in origin (*3*–*6*). The dark bands appear to be flat-lying in many areas at the 10-m scale. Many of the dark-toned bands consist of a mixture of meter-scale boulders of light-toned material and finer-grained dark material (figs. S3 and S4). The patches of fine-grained dark material commonly have a hummocky texture that is consistent with ripples of ~2 to 5 m in wavelength (fig. S3). Evidence of recent eolian activity is pervasive throughout the scene [supporting online material (SOM) text]. Therefore, this flat-lying dark material is interpreted as surficial deposits of sediment composed of eolian sand, with a possible component of lag. Dark material within the underlying bedrock may also contribute to the tone of the dark bands.

The source of the dark-toned sediment is unconstrained by the present study, but it may be present within the underlying bedrock and became mobilized through eolian erosion or persists in place as lag deposits. Dark material may also have been transported from a distal source.

Local topography and high surface roughness of select layers within the light-toned bedrock apparently contribute to the accumulation of the dark sediment in distinct bands (figs. S3 to S5). The dark-toned bands are commonly found within topographic depressions in the underlying bedrock. Accumulations of boulders also act to trap dark-toned sediment within the bands (SOM text). Thus, the dark-toned bands appear to consist of sediment that has accumulated within the troughs between ridges of light-toned bedrock.

This ridge-and-trough morphology is consistent with differential erosion, which can be

Lunar and Planetary Laboratory, University of Arizona, Tucson, AZ 85721, USA.

*To whom correspondence should be addressed. E-mail: chriso@lpl.arizona.edu